Research Article

Mitsunori Toyoda*

Flat-field anastigmatic mirror objective for high-magnification extreme ultraviolet microscopy

DOI 10.1515/aot-2015-0020
Received March 9, 2015; accepted May 8, 2015; previously published online June 4, 2015

Abstract: To apply high-definition microscopy to the extreme ultraviolet (EUV) region in practice, i.e. to enable *in situ* observation of living tissue and the at-wavelength inspection of lithography masks, we constructed a novel reflective objective made of three multilayer mirrors. This objective is configured as a two-stage imaging system made of a Schwarzschild two-mirror system as the primary objective and an additional magnifier with a single curved mirror. This two-stage configuration can provide a high magnification of 1500, which is suitable for real-time observation with an EUV charge coupled device (CCD) camera. Besides, since off-axis aberrations can be corrected by the magnifier, which provides field flattener optics, we are able to configure the objective as a flat-field anastigmatic system, in which we will have a diffraction-limited spatial resolution over a large field-of-view. This paper describes in detail the optical design of the present objective. After calculating the closed-form equations representing the third-order aberrations of the objective, we apply these equations to practical design examples with a numerical aperture of 0.25 and an operation wavelength of 13.5 nm. We also confirm the imaging performances of this novel design by using the numerical ray-tracing method.

Keywords: aberration theory; extreme ultraviolet; microscopy; multilayer mirror; soft X-ray.

***Corresponding author: Mitsunori Toyoda,** Institute of Multidisciplinary Research for Advanced Materials, Tohoku University, Sendai 980-8577, Japan,
e-mail: toyoda@tagen.tohoku.ac.jp

www.degruyter.com/aot
© 2015 THOSS Media and De Gruyter

1 Introduction

Researchers in extreme ultraviolet (EUV) and soft X-ray optics aim to develop an imaging system that can focus these types of light and form an image with diffraction-limited spatial resolution. In particular, there has been a growing demand for a microscope objective for applications in the shorter wavelength region, intended for *in situ* observation of living tissue [1–3], defect inspection of lithography masks [4–6], and intense-field generation with higher harmonics and free-electron lasers [7, 8]. Because of the high absorption of optical materials, traditional lenses cannot be used in the EUV region. Instead, objectives based on a diffractive zone plate and reflective multilayer mirrors have been investigated. To achieve EUV and soft X-ray microscopy with high resolution, there are two main technical challenges associated with the objective. First, the objective should have high magnification. We shall consider the case of the characterization of fine structures at a scale of a few tens of nanometers, which corresponds to organelles in living cells or defects on lithography masks, using a full-field microscope. Since the pixel size of common two-dimensional detectors for use in the EUV region, i.e. CCD cameras and microchannel plates, ranges between 10 and 50 μm, the objective should form an enlarged image at a high magnification of 500–2000 on the detector for the detection of fine structures. Secondly, aberrations of the objective should be corrected and reduced to an extremely small value for diffraction-limited imaging, so as to eliminate image blurring. According to Maréchal [9], the allowable wave aberration of the objective operating at a wavelength of 13.5 nm drops to 1 nm root mean square (rms), for example.

A diffractive zone plate is a notable instance of an objective satisfying these two requirements of EUV microscopy. Wave diffraction occurring on a concentric grating on a flat transparent membrane enables the zone plate to act as a focusing or imaging element under high magnification. Moreover, by using wave optics theory [10], the grating patterns can be designed to correct spherical aberrations, where blur-free imaging with diffraction-limited

resolution would be expected near the optical axis. On the other hand, it is also known that a zone plate cannot correct off-axis aberrations in the Seidel theory, i.e. coma and astigmatism, since a zone plate does not have a sufficient degree of freedom in its design space to correct these aberrations. Typically, the imaging of objects several micrometers away from an optical axis would result in blurring because of these off-axis aberrations.

An optical system consisting of reflective multilayer mirrors is another instance of an objective with better correction of the off-axis aberrations. The Schwarzschild objective, a representative two-mirror objective for microscopy, can be configured to correct the first three Seidel aberrations, i.e. spherical aberration, coma, and astigmatism, to be an anastigmatic system [11–14]. As image blur for objects several tens of micrometers away from an optical axis can be remarkably low, diffraction-limited imaging would be expected to be possible in a wider field-of-view with the Schwarzschild design. In contrast to a zone plate, however, this mirror objective has practical limitations on achieving a high magnification. Horikawa et al. has demonstrated a Schwarzschild objective with a magnification of 200 [15]. However, it has also been shown that as the magnification increases, the system will have to consist of very small multilayer mirrors with diameters of a few millimeters, which are very difficult to fabricate. This practical limitation on the magnification necessitates a two-dimensional detector with a pixel size of <1 μm, i.e. a photographic film or an electron-zooming tube [16], for diffraction-limited imaging, where the quantum efficiency would be fairly reduced or observations would be restricted to still images by the need for off-line development. To overcome these limitations in existing microscope objectives, we have recently proposed a novel objective design consisting of three multilayer mirrors [17]. It simultaneously achieves high magnification and good correction of the off-axis aberrations. This novel objective has been used for the observation of an EUV lithography mask at a wavelength of 13.5 nm [18]. By combining this objective and a CCD camera, we have demonstrated full-field EUV images of lithography masks with near diffraction-limited resolution, where fine line and space patterns with a half pitch down to 30 nm were clearly resolved [19]. In this paper, we provide a detailed description of the optical design process for this three-mirror objective. First, we derive closed-form representations for the imaging aberrations in a three-mirror imaging system to the third order. Then, the closed-form equations were used to design an objective for high-magnification EUV microscopy with good correction of the off-axis aberrations. In our design example, a magnification of 1500 for a wavelength of 13.5 nm were taken as typical parameters. Finally, design performances including high resolution over a large field-of-view were confirmed by the numerical ray tracing method.

2 Third-order aberration coefficients for the three-mirror objective

2.1 Notations

In this section, we calculate the aberration coefficients for a microscope objective consisting of three multilayer mirrors in a finite conjugate. The objective is configured as a two-stage imaging system made of a primary two-mirror objective, i.e. the Schwarzschild design, and an additional magnifier consisting of a single curved mirror. For an easy understanding of the aberrations observed on a sample plane of a full-field microscope, we treat the optics in reverse order so as to produce a demagnification system. Employing a standard configuration and notations used in optical design [20], the imaging system consists of an object plane (i=0), an additional magnifier (i=1), an intermediate image plane (i=2), a primary objective (i=3 and 4), and a final image plane (i=5), as shown schematically in Figure 1. The optical axis is taken as x in Cartesian coordinates with an object located on the y–z plane. The surface figure of the mirrors can be represented by the following formula, employing a fourth-order deformation coefficient, b_i, modifying the radius of the i-th mirror curvature, r_i, in the form

$$x_i = \frac{y_i^2 + z_i^2}{2r_i} + \frac{1}{8}\left(\frac{1}{r_i^3} + b_i\right)(y_i^2 + z_i^2)^2, \tag{1}$$

where (x_i, y_i, z_i) are the coordinates with the mirror vertex taken as the origin. We also introduce the following quantities:

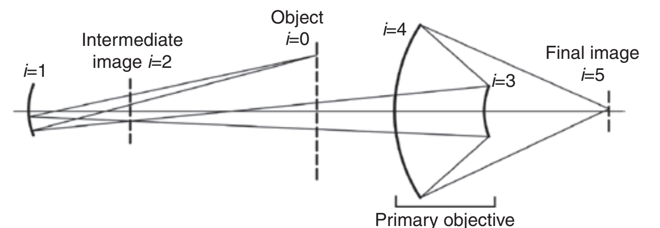

Figure 1: Schematic drawing for the three-mirror objective. The objective is made of an additional magnifier with a single element (i=1) and the primary objective with two mirrors (i=3, 4).

m: lateral magnification of the whole imaging system,
m_p: lateral magnification of the primary objective,
d_i: distance between the i-th and (i+1)-th items in Figure 1 (i=0–4),
N_i: refractive index of the medium traversed by the ray while traveling from the (i-1)-th item to the i-th item in Figure 1 (i=1–5). The refractive indices are set to +1 or -1 [21], depending on whether the direction of the ray travel along the x axis is positive or negative, respectively:

$$N_1=N_4=-1,\quad N_2=N_3=N_5=1. \tag{2}$$

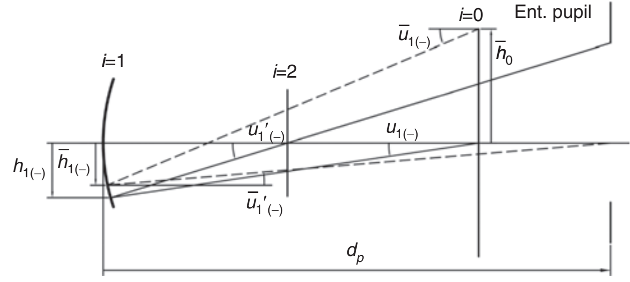

Figure 2: Generalized single-mirror configuration for the additional magnifier. u_i and $\bar{u}_i$ in the figure represent inclination angles of the marginal and chief rays, respectively.

2.2 Derivation of third-order aberration coefficients

A lateral aberration on the image plane for an object that has a Gaussian image height, R, is given in terms of five Seidel coefficients for the y direction as

$$\Delta_y=-\frac{1}{2}[I\cdot NA^3\cos\varphi+II\cdot R\cdot NA^2(2+\cos 2\varphi) +(3III+P)R^2\cdot NA\cos\varphi+V\cdot R^3], \tag{3}$$

and for the z direction as

$$\Delta_z=-\frac{1}{2}[I\cdot NA^3\sin\varphi+II\cdot R\cdot NA^2\sin 2\varphi+(III+P)R^2\cdot NA\sin\varphi], \tag{4}$$

where I, II, III, P, and V denote the coefficients for the spherical aberration, coma, astigmatism, Petzval sum representing field curvature, and distortion, respectively. The polar coordinate (NA, φ) of the pupil is expressed by the numerical aperture, NA, in the image plane, while the angle φ is measured from the y-axis in the direction of the z-axis. In this report, the first four aberration coefficients, I, II, III, and P, are considered since image blurring should come from these aberration terms. The term of distortion, which is proportional to the cube of the image height but independent of the numerical aperture, should not introduce an image blur, so that we disregard the effects of distortion in the following analysis. These aberration coefficients for the whole system can be calculated by summing up the contributions of the primary objective and the additional magnifier. As the coefficients for the primary objective have already been studied minutely in previous papers [22, 23], we calculate the aberrations of the additional magnifier in the following analysis.

The aberration coefficients of the additional magnifier can be calculated by tracing two paraxial rays, a marginal ray and a chief ray, shown with solid and dashed lines, respectively, in Figure 2. On the basis of reference [20], general solutions to the third-order aberration coefficients for the i-th optical element can be obtained:

$$I_i=h_i(h_iQ_i)^2\left[h_i\Delta\left(\frac{1}{Ns}\right)_i\right]+h_i^4\psi_i, \tag{5}$$

$$II_i=h_i(h_iQ_i)(\bar{h}_i\bar{Q}_i)\left[h_i\Delta\left(\frac{1}{Ns}\right)_i\right]+h_i^3\bar{h}_i\psi_i, \tag{6}$$

$$III_i=h_i(\bar{h}_i\bar{Q}_i)^2\left[h_i\Delta\left(\frac{1}{Ns}\right)_i\right]+h_i^2\bar{h}_i^2\psi_i, \tag{7}$$

$$P_i=\frac{N_{i+1}-N_i}{N_iN_{i+1}r_i}. \tag{8}$$

In these equations, auxiliary quantities are defined for simplicity as

$$h_iQ_i=h_i\frac{N_i}{r_i}-\alpha_i, \tag{9}$$

$$\bar{h}_i\bar{Q}_i=\bar{h}_i\frac{N_i}{r_i}-\bar{\alpha}_i, \tag{10}$$

$$h_i\Delta\left(\frac{1}{Ns}\right)_i=\frac{\alpha_{i+1}}{N_{i+1}^2}-\frac{\alpha_i}{N_i^2}, \tag{11}$$

$$\psi_i=(N_{i+1}-N_i)b_i, \tag{12}$$

where h_i and α_i represent the height and the reduced angle of the incident ray, calculated by tracing the paraxial marginal ray through the system, while $\bar{h}_i$ and $\bar{\alpha}_i$ are the corresponding values for the chief ray. The reduced angle is given by multiplying the inclination angle of the rays by the refractive index of the medium.

Next, we will transform the set of general equations above for the additional magnifier.

The procedure involves calculating the two paraxial rays with the following ray-tracing equations to the first order:

$$h_{i+1}=h_i-\frac{d_i}{N_{i+1}}\alpha_{i+1}, \tag{13}$$

$$\alpha_{i+1}=\alpha_i+\phi_i h_i, \tag{14}$$

where ϕ_i denotes the refractive power defined as the inverse of the focal length, f_i, of the i-th element:

$$\phi_i\equiv\frac{1}{f_i}=\frac{N_{i+1}-N_i}{r_i}. \tag{15}$$

For the marginal ray, we have the following relationships:

$$h_0=h_2=h_4=0, \tag{16}$$

$$\alpha_1=m, \tag{17}$$

$$\alpha_2=m_p, \tag{18}$$

$$\alpha_5=1. \tag{19}$$

Substituting equations (2) and (16)–(18) into equations (13) and (14), we get:

$$h_1=\frac{m_p-m}{\phi_1}, \tag{20}$$

$$d_0=\frac{m_p-m}{m\phi_1}, \tag{21}$$

$$d_1=\frac{m_p-m}{m_p\phi_1}. \tag{22}$$

For easy calculation of the parameters related to the chief ray, we introduce the entrance pupil of the primary objective, which is a separated from the additional magnifier by a distance, d_p. From the definition of the chief ray, we have

$$\bar{h}_0=\frac{1}{m}, \tag{23}$$

$$\bar{h}_p=0, \tag{24}$$

$$\bar{h}_5=1, \tag{25}$$

where $\bar{h}_p$ represents the height of the chief ray on the entrance pupil. For the chief ray, we combine equations (13), (14), (23) and (24) to obtain:

$$\bar{h}_1=\frac{d_p\phi_1}{m_p-m+d_pm_p\phi_1}, \tag{26}$$

$$\bar{\alpha}_1=\frac{\phi_1(1+d_p\phi_1)}{m_p-m+d_pm_p\phi_1}, \tag{27}$$

$$\bar{\alpha}_2=-\frac{\phi_1}{m_p-m+d_pm_p\phi_1}. \tag{28}$$

By introducing the following practical approximations, we can simplify the above expressions pertaining to the chief ray for the case of a high-magnification objective. We assume that the magnification of the whole system is much smaller than that of the primary objective, i.e.

$$|m|<<|m_p|<1, \tag{29}$$

while the distance between the magnifier and the pupil, d_p, should be much larger than the focal length of the magnifier, f_1, i.e.

$$\left|\frac{d_p}{f_1}\right|=|d_p\phi_1|>>1. \tag{30}$$

Substituting equations (29) and (30) into equations (26)–(28) yields the following approximate functions:

$$\bar{h}_1=1/m_p, \tag{31}$$

$$\bar{\alpha}_1=-\phi_1/m_p, \tag{32}$$

$$\bar{\alpha}_2=0. \tag{33}$$

Note that the suitability of these two approximations will be discussed using design examples in the next section.

Finally, the aberration coefficients of the additional magnifier (i=1) can be calculated by substituting equations (2), (15)–(18), (20), and (31)–(33) into equations (5)–(12), which yields

$$I_1=\frac{(m^2-m_p^{\,2})^2}{4\phi_1}+\frac{2(m-m_p)^4}{\phi_1^{\,4}}b_1, \tag{34}$$

$$II_1=-\frac{(m-m_p)^2(m+m_p)}{4m_p}-\frac{2(m-m_p)^3}{m_p\phi_1^{\,3}}b_1, \tag{35}$$

$$III_1=\frac{(m-m_p)^2\phi_1}{4m_p^{\,2}}+\frac{2(m-m_p)^2}{m_p^{\,2}\phi_1^{\,2}}b_1, \tag{36}$$

$$P_1=-\phi_1. \tag{37}$$

Equations (34)–(37) show that the aberration coefficients of the additional magnifier can be described by two independent design parameters, *viz.*, the refractive power, ϕ_1, and the deformation coefficient, b_1, of the first mirror, for a given magnification of the whole imaging system, m, and of the primary objective, m_p.

3 Design examples of high-magnification objective

The following design examples demonstrate how the aberration coefficients derived in the previous section can be applied to the design of high-magnification objectives with good correction of off-axis aberrations. We consider EUV objectives having a magnification, m, of 1/1500, a numerical aperture, NA, of 0.25, and an operating wavelength of 13.5 nm. The Schwarzschild objective in our previous paper [23], which has a magnification m_p=-1/50, is employed as the primary objective. The construction parameters for the Schwarzschild objective consisting of two spherical mirrors, i.e. the radii of curvature and mirror separations, are listed in Table 1. We only consider the Petzval sum, P_p, as a residual aberration arising from the primary objective, since the other aberration terms, i.e. spherical aberration, coma, and astigmatism, vanish in the Schwarzschild design, as shown in Table 2.

Now we shall treat the case where the additional magnifier is made of a spherical mirror, i.e. b_1=0, as a practical example (design A). In this case, equations (34)–(37) indicate that we have one independent parameter, i.e. the refractive power, ϕ_1, in the design space of the high-magnification objective, and there is a possibility to

Table 1: Construction parameters for the design examples of the three-mirror objective.

Radius of curvature	r_1 (mm)	38.447
	r_3 (mm)	24.286
	r_4 (mm)	65.935
Mirror deformation	b_1 (m^{-3})	-1.76×10^4
Separation distance	d_0 (mm)	-595.93
	d_1 (mm)	19.864
	d_2 (mm)	956.106
	d_3 (mm)	-41.624
	d_4 (mm)	85.607

For the Schwarzschild objective, the parameters were derived by third-order theory [23], except for the mirror separations d_3 and d_4, which were slightly modified to reduce higher-order spherical aberration.

Table 2: Third-order aberration coefficients for the design examples, and corresponding lateral aberrations computed on the final image plane.

	Design A	Design B	Schwarzschild
Spherical aberration *I*	7.67×10^{-10}	-1.09×10^{-8}	0
Lateral aberration (nm)	<0.1	<0.1	0
Coma *II*	-1.03×10^{-4}	-2.14×10^{-4}	0
Lateral aberration (nm)	1.1	2.0	0
Astigmatism *III*	13.9	0	0
Petzvar *P*	0	0	52.0
Lateral aberration M (nm)	104.2	0	130.1
Lateral aberration S (nm)	34.7	0	130.1

Values for the Schwarzschild design are also shown as the reference.

correct one of the four aberrations in these equations by varying ϕ_1 as a design parameter. To achieve a wide field of view, an efficient use of the limited design parameter is to reduce the Petzval sum by using the additional magnifier as field flattener optics [24]. To reduce the Petzval sum, we need

$$P=P_p+P_1=0. \tag{38}$$

Then, by substituting equation (37) into equation (38), the design parameter ϕ_1 becomes

$$\phi_1=P_p. \tag{39}$$

The construction parameters for the additional magnifier can be calculated by combining equations (15), (21)–(22), and (39). The results are tabulated in Table 1. To compensate for reducing the Petzval sum, other aberrations, *viz.*, spherical aberration, coma, and astigmatism, must arise in the spherical system. We estimate the effects of these residual aberrations by computing the lateral aberrations on the image plane. By substituting the aberration coefficients of equations (34)–(36) into equations (3)–(4), we get the lateral aberrations for an off-axis object with an image height, R, of 100 μm, as summarized in column 'Design A' of Table 2. The coefficients for the spherical aberration and coma were of the order of 10^{-4}–10^{-10}, and the corresponding lateral aberrations on the image plane were confirmed to be 1 nm or less, which is negligibly small compared to the Rayleigh resolution of the objective, i.e. 33 nm. In contrast, astigmatism has the dominant effect on the spherical system. We observed a relatively large lateral aberration of 104 nm on a meridional plane (φ=0°), while one-third of that value was obtained on a sagittal plane (φ=90°). As a result of the field flattening effect of the additional magnifier, however, these lateral aberrations are expected to be smaller than those for the Schwarzschild objective on both the meridional and sagittal planes.

Further correction of the aberrations would be expected to occur upon introducing an aspherical surface to the additional magnifier, i.e. $b_1 \neq 0$ (design B). Since there are two independent parameters, *viz.*, the deformation coefficient, b_1, and the refractive power, ϕ_1, in the design space of the aspherical system, we can correct not only the Petzval sum by satisfying equation (39), but also the astigmatism, which dominates the aberrations of the spherical system above, by optimizing the deformation coefficient. Substituting equation (39) into equation (36), we obtain the condition for correction of the astigmatism:

$$III_1 = \frac{(m-m_p)^2 P_p}{4m_p^{\ 2}} + \frac{2(m-m_p)^2}{m_p^{\ 2} P_p^{\ 2}} b_1 = 0, \tag{40}$$

which yields

$$b_1 = -P_p^{\ 3} / 8. \tag{41}$$

The numerical value for the deformation coefficient is shown in Table 1. The coefficients of residual aberrations can be obtained by substituting equations (39) and (41) into equations (34) and (35). The lateral aberrations for these residual terms, i.e. spherical aberration and coma, were also computed, as shown in the 'Design B' column of Table 2. The coefficients were of the order of 10^{-4}–10^{-8}, and the corresponding lateral aberrations still had negligibly small values below 2 nm. This result clearly indicated that the first four Seidel aberrations to the third order, i.e. spherical aberration, coma, astigmatism, and Petzval sum, can be sufficiently corrected by introducing the aspherical magnifier. Thus, we were able to configure the three-mirror objective as a flat-field anastigmatic system with a very large field-of-view.

Finally, the imaging properties of the design examples above were confirmed with exact numerical calculations. We applied the ray-tracing software CodeV (Synopsys, Inc., Pasadena, CA, USA) [25] in the following computations. Figure 3 shows spot diagrams observed on the final image plane for both design examples. As a reference, the results for the Schwarzschild objective are also provided. For an on-axis object, we observed almost the same diagrams in all designs. This suggested that the aberrations for the on-axis object were due to the Schwarzschild objective and that the additional magnifier had little effect. The above results are also consistent with the fact that the spherical aberration of the magnifier was negligibly small in both examples. When the image height increased, the image blur expanded in design A, as shown in Figure 3A. For the 100-µm-high object, we

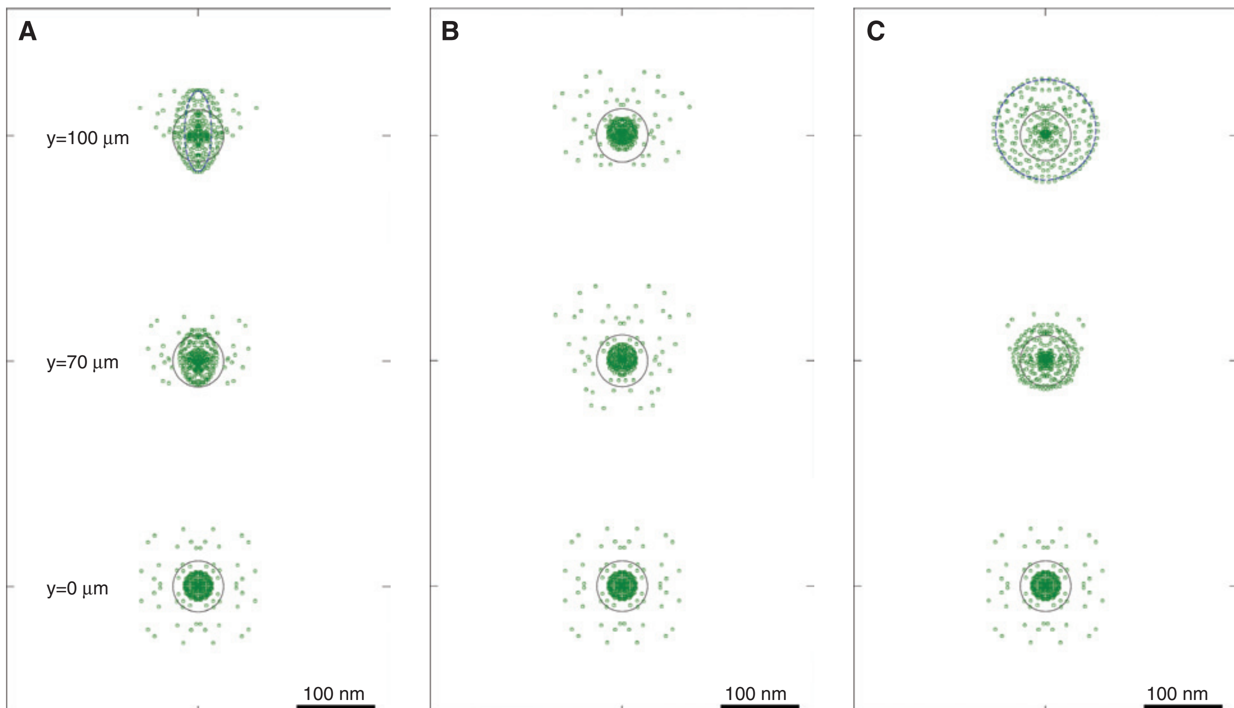

Figure 3: Spot diagrams calculated on the final image plane. (A) design A with spherical magnifier, (B) design B with aspherical magnifier, (C) Schwarzschild design. Vignetting effects were ignored in computations. Solid circles indicate the Airy disk that represents diffraction-limited resolution.

clearly observed the blur of an elliptical shape, which is typical in imaging with astigmatism. Besides, the locus of the lateral aberration, calculated by using equations (3) and (4) (shown with a blue dashed ellipse in Figure 3A), coincided fairly well with the spot diagram. In addition to showing the quantitative exactness of the closed-form representations derived above, this result suggests that the approximations given by equations (29) and (30) are adequate in the three-mirror imaging system with high magnification. In design B, further correction of the off-axis aberrations was clearly observed. We confirmed that almost the same spot diagrams were obtained regardless of the image height, as shown in Figure 3B. Moreover, the spot diagrams were nearly isotropic for all image heights. These two facts imply that the aberrations of asymmetry, i.e. coma and astigmatism, should be sufficiently reduced and that the objective should have a flat imaging field.

To quantify the field-of-view of the objectives, the Strehl definition was calculated as a function of the image height, as shown in Figure 4. According to Maréchal, an imaging system should have a Strehl definition of over 0.8 for diffraction-limited imaging [9], and we can estimate the field-of-view of our design examples by applying this criterion. In design A, made of spherical mirrors, we confirmed that diffraction-limited imaging can be achieved in an extended field-of-view. The criterion was satisfied at an image height below 80 μm, which is 30% higher than that for the Schwarzschild design, i.e. 60 μm. In the case of design B, which introduced the aspherical magnifier, the Strehl definition hardly depended on the image height below 100 μm, slowly reaching the threshold at an image height of 270 μm. This clearly demonstrated that the off-axis aberrations are eliminated efficiently in the proposed flat-field anastigmatic mirror objective, and that high-magnification EUV microscopy with diffraction-limited resolution can be expected over a fairly large field-of-view, about 20 times larger than that for the Schwarzschild design.

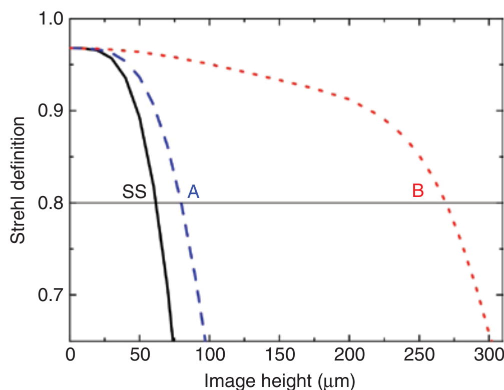

Figure 4: Strehl definition as a function of image height on the final image plane. According to Maréchal, a Strehl definition above 0.8 would be required for diffraction-limited imaging. To avoid obstruction of light rays to the primary objective on the object plane (i=0), we can place an object in the annular area that has an image height of over 3 μm.

4 Summary

To enable the use of high-definition imaging in practical applications in the extreme ultraviolet region, i.e. for *in situ* observation of living tissue and at-wavelength inspection of lithography masks, there has been a growing demand for a wide-field microscope enabling real-time characterization with diffraction-limited spatial resolution. In this paper, we propose a novel reflective objective made of three multilayer mirrors and describe the optical design of this objective by demonstrating the high magnification required for real-time observation with a CCD camera and good correction of off-axis aberrations yielding a large field-of-view. First, we consider a two-stage imaging system consisting of a Schwarzschild mirror as a primary objective and an additional magnifier made of a single curved mirror. Then, the imaging aberrations for this system are calculated and represented in terms of closed-form equations by using third-order theory. Secondly, these equations are applied to design high-magnification objectives that have a magnification of 1500, a numerical aperture of 0.25, and an operational wavelength of 13.5 nm. We report two design examples. One features a magnifier made of a spherical surface, where we correct the Petzval sum by accepting a small astigmatism. In our second example with an aspherical magnifier, we correct the first four Seidel aberrations and demonstrate a flat-field anastigmatic objective by optimizing the extended design parameters of the magnifier. Finally, the imaging performance of these design examples is computed by applying the numerical ray-tracing method. We confirm the extended field-of-view in both examples. Particularly in the aspherical design, we clearly demonstrate that a diffraction-limited resolution of 33 nm would be expected in a wide field-of-view with a diameter of 540 μm.

To be able to construct a wide-field microscope based on the proposed three-mirror objective, a very large-scale CCD camera would be required as a two-dimensional detector. Such detectors have been reported during the development of large astronomical telescopes, including the Suprime-Cam camera for the Subaru telescope [26], which has 8000 mega pixels over a diameter of 200 mm.

These techniques for large-scale CCD cameras can be applied to the EUV region, and the proposed objective would be key to realizing a wide-field microscope for applications in various research fields including the life sciences, materials science, and the semiconductor industry, where the capability for multi-scale imaging is an essential requirement.

Funding: Japan Society for the Promotion of Science, (Grant/Award Number: KAKENHI/22760020; KAKENHI/25390088), Japan Science and Technology Agency, (Grant/Award Number: Research Seeds Quest Program).

References

[1] W. L. Chao, B. D. Harteneck, J. A. Liddle, E. H. Anderson and D. T. Attwood, Nature 435, 1210 (2005).
[2] K. Jefimovs, J. Vila-Comamala, T. Pilvi, J. Raabe, M. Ritala, et al., Phys. Rev. Lett. 99, 264801 (2007).
[3] Y. Horikawa, K. Nagai, S. Mochimaru and Y. Iketaki, J. Microsc. 172, 189 (1993).
[4] K. A. Goldberg, A. Barty, Y. Liu, P. Kearney, Y. Tezuka, et al., J. Vac. Sci. Technol. B 24, 2824 (2006).
[5] K. Hamamoto, Y. Tanaka, T. Yoshizumi, N. Hosokawa, N. Sakaya, et al., Jpn. J. Appl. Phys. 45, 5378 (2006).
[6] K. Takase, Y. Kamaji, N. Sakagami, T. Iguchi, M. Tada, et al., Jpn. J. Appl. Phys. 49, 06GD07 (2010).
[7] E. J. Takahashi, Y. Nabekawa, H. Mashiko, H. Hasegawa, A. Suda, et al., IEEE J. Sel. Top. Quantum Eelectron. 10, 1315 (2004).
[8] H. Fukuzawa, X.-J. Liu, G. Prümper, M. Okunishi, K. Shimada, et al., Phys. Rev. A 79, 031201(R) (2009).
[9] M. Born and E. Wolf, in Principles of Optics (Pergamon Press, Oxford, 1980) Chap. 9.3.
[10] L. N. Hazra, Y. Han and C. A. Delisle, J. Mod. Opt. 40, 1531 (1993).
[11] P. Erdös, J. Opt. Soc. Am. 49, 877 (1959).
[12] A. A. Malyutin, Quantum Electronics 27, 90 (1997).
[13] A. A. Malyutin, Quantum Electronics 27, 182 (1997).
[14] S. Bollanti, P. Di Lazzaro, F. Flora, L. Mezi, D. Murra, et al., Appl. Phys. B 91, 127 (2008).
[15] Y. Horikawa, S. Mochimaru, Y. Iketaki, K. Nagai, K. Okawa, et al., Proc. SPIE 1720, 217 (1992).
[16] T. Haga, H. Kinoshita, K. Hamamoto, S. Takada, N. Kazui, et al., Jpn. J. Appl. Phys. 42, 3771 (2003).
[17] M. Toyoda, Japanese Patent No. 5489034 (2009).
[18] M. Toyoda, K. Yamasoe, T. Hatano, M. Yanagihara, A. Tokimasa, et al., Appl. Phys. Express 5, 112501 (2012).
[19] M. Toyoda, K. Yamasoe, A. Tokimasa, K. Uchida, T. Harada, et al., Appl. Phys. Express 7, 102502 (2014).
[20] Y. Matsui and K. Nariai, in Fundamentals of Practical Aberration Theory (World Scientific, Singapore, 1993) Chap. 1.2.
[21] V. N. Mahajan, in Optical Imaging and Aberrations (SPIE Press, Washington, 1998) Part 1, Chap. 1.3.7.
[22] M. Toyoda and M. Yamamoto, Opt. Rev. 13, 149 (2006).
[23] M. Toyoda, Opt. Rev. 18, 441 (2011).
[24] V. N. Mahajan, in Optical Imaging and Aberrations (SPIE Press, Washington, 1998) Part 1, Chap. 5.11.
[25] CodeV, Home page URL: http://optics.synopsys.com/codev/.
[26] S. Miyazaki, Y. Komiyama, M. Sekiguchi, S. Okamura, M. Doi, et al., Publ. Astron. Soc. Japan 54, 833 (2002).

Mitsunori Toyoda
Institute of Multidisciplinary Research for Advanced Materials, Tohoku University, Sendai 980-8577, Japan,
toyoda@tagen.tohoku.ac.jp

Mitsunori Toyoda is an Assistant Professor at the Center for Advanced Microscopy and Spectroscopy, IMRAM, Tohoku University, Japan. He was born and raised in Tokyo. He received his Bachelor's degree, Master's degrees, and PhD, all in Engineering, from Tohoku University. After working at Nikon as an optical designer, he joined IMRAM, Tohoku University, in 2004. His current interests include optical design, instrumentation, and application of EUV microscopy based on multilayer-mirror imaging systems.